10/4-4-97 JSD

SANDIA REPORT

SAND96-8253 • UC–1409
Unlimited Release
Printed August 1996

M9705238 2

Heat Transfer and Flow Stability in a Rotating Disk/Stagnation Flow Chemical Vapor Deposition Reactor

S. Joh, G. H. Evans

Prepared by
Sandia National Laboratories
Albuquerque, New Mexico 87185 and Livermore, California 94551
for the United States Department of Energy
under Contract DE-AC04-94AL85000

DISCLAIMER

UC-1409

SAND96-8253
Unlimited Release
Printed August 1996

Heat Transfer and Flow Stability in a Rotating Disk/Stagnation Flow Chemical Vapor Deposition Reactor

S. Joh †

G. H. Evans

Thermal and Plasma Processes Department
Sandia National Laboratories, Livermore, CA 94551–0969

ABSTRACT

The flow and heat transfer in a vertical high-speed rotating disk/stagnation flow chemical vapor deposition (CVD) reactor is studied with particular emphasis on the effects of the spacing, $\overline{H}$, between the stationary gas inlet and the rotating disk. A one-dimensional analysis is used to determine the effects of $\overline{H}$, flow rate, and disk spin rate on the gas flow patterns and the heat transfer from the disk; the effects of buoyancy, reactor side walls, and finite disk geometry (reactor radius $\overline{r}_o$, rotating disk radius $\overline{r}_d$) on these quantities are determined in a two-dimensional analysis. The Navier-Stokes and energy equations are solved for hydrogen over a range of gas flow rates, disk spin rates, axial and radial aspect ratios, for a pressure of 250 Torr, inlet gas temperature of 50 C, and disk temperature of 800 C (dimensionless parameters are the disk Reynolds number, $\mathrm{Re}_\omega = \overline{r}_d{}^2\overline{\omega}/\overline{\nu}_{\mathrm{in}}$, the mixed convection parameter $\mathrm{Gr}/\mathrm{Re}_\omega{}^{3/2}$ where $\mathrm{Gr} = \overline{g}\,(\overline{\rho}_{\mathrm{in}} - \overline{\rho}_d)\,\overline{r}_d{}^3/(\overline{\rho}_{\mathrm{in}}\overline{\nu}_{\mathrm{in}}{}^2)$, the dimensionless inlet velocity $\mathrm{SP} = |\overline{u}_{\mathrm{in}}|/\sqrt{\overline{\omega}\,\overline{\nu}_{\mathrm{in}}}$, the Prandtl number $\mathrm{Pr} = \overline{\nu}_{\mathrm{in}}/\overline{\alpha}_{\mathrm{in}}$, and variable property ratios). The 1D similarity solution results show that the dimensionless heat transfer from the rotating disk, Nu_{1D}, depends on SP and Re_ω to a much greater extent at smaller spacings ($A = \overline{H}/\overline{r}_d = 0.54$) than at larger spacings ($A = 2.16$). For SP values of 0.92 and 4.5 and for both spacings studied ($A = 0.54$ and 2.16), Nu_{1D} approaches the value for an infinite rotating disk for $\mathrm{Re}_\omega \approx 450$, except for the case at SP=4.5 and $A = 0.54$ where Nu_{1D} is significantly larger. The 1D results also show that for small SP (0.23) there is a significant flow toward $r = 0$ (the radial component of velocity is negative) which is larger for the smaller value of A. The 2D results show that the effect of inlet velocity (SP) on the radial variation of the disk heat transfer (Nu_{2D}) is greater for larger values of A; for both values of A there is greater radial variation of Nu_{2D} at the larger value of SP. At the larger

A, the radial uniformity of Nu_{2D} is improved significantly when the inlet velocity matches the asymptotic value for an infinte rotating disk. For both values of A there is gas recirculation above the rotating disk when the disk is "starved" (SP=0.23, Re_ω=456); for A=0.54 the thermal boundary layer extends to the gas inlet and Nu_{2D} is uniform. The uniformity of Nu_{2D} and the recirculation of the gas above the disk were only slightly affected when $\overline{r}_o/\overline{r}_d$ was varied by approximately 30% (from 1.1 to 1.4) for the conditions SP=0.23, A=0.54, and Re_ω=456.

† currently at Novellus, San Jose, CA.

1 Nomenclature

A	axial aspect ratio, $\overline{\mathrm{H}}/\overline{r}_d$
Gr	Grashof number, $\overline{g}\,(\overline{\rho}_{\mathrm{in}}-\overline{\rho}_d)\overline{r}_d{}^3/(\overline{\rho}_{\mathrm{in}}\overline{\nu}_{\mathrm{in}}{}^2)$
$\mathrm{Gr}/\mathrm{Re}_\omega{}^{3/2}$	mixed convection parameter (MCP), $\overline{g}\,(\overline{\rho}_{\mathrm{in}}-\overline{\rho}_d)/(\overline{\rho}_{\mathrm{in}}\overline{\nu}_{\mathrm{in}}^{1/2}\overline{\omega}^{3/2})$
$\overline{\mathrm{H}}$	disk to inlet distance
$\overline{\mathrm{L}}$	disk to outlet distance
Nu	Nusselt number, $-\left(k\frac{\partial\Theta}{\partial x}\right)\Big\vert_{x=0}$
Pr	Prandtl number, $\overline{\nu}_{\mathrm{in}}/\overline{\alpha}_{\mathrm{in}}$
Re_ω	disk Reynolds number, $\overline{r}_d{}^2\overline{\omega}/\overline{\nu}_{\mathrm{in}}$
$\mathrm{Re}_{\mathrm{in}}$	inlet Reynolds number, $\lvert\overline{u}_{\mathrm{in}}\rvert\,\overline{\mathrm{H}}/\overline{\nu}_{\mathrm{in}}$
SP	flow parameter, $\lvert\overline{u}_{\mathrm{in}}\rvert/\sqrt{\overline{\omega}\,\overline{\nu}_{\mathrm{in}}}$
$\overline{T}$	temperature
c_p	specific heat at constant pressure
f	ratio w/r
k	thermal conductivity
p_m	pressure in momentum equations
r	radial coordinate
$\overline{r}_d$	disk radius
$\overline{r}_o$	reactor radius
u	axial velocity component
v	radial velocity component
w	circumferential velocity component
x	axial coordinate

1.1 Greek symbols

α	thermal diffusivity, $k/(\rho c_p)$
ϵ	temperature ratio, $(\overline{T}_d-\overline{T}_{\mathrm{in}})/\overline{T}_{\mathrm{in}}$
ρ	density
ν	kinematic viscosity, μ/ρ
Θ	dimensionless temperature, $(\overline{T}-\overline{T}_{\mathrm{in}})/(\overline{T}_d-\overline{T}_{\mathrm{in}})$
μ	dynamic viscosity
ω	disk spin rate

1.2 Subscripts and superscripts

$_d$ disk quantity

$^-$ dimensional quantity

$_{\text{ref}}$ reference quantity

$_{\text{1D}}$ one-dimensional solution quantity

$_{\text{2D}}$ two-dimensional solution quantity

$_{\text{in}}$ evaluated at reactor inlet

2 Introduction

Uniform growth of materials on substrates is one of the primary reactor design objectives in microelectronics materials manufacturing. The uniformity depends in a complex way on the gas flow (forced and buoyancy-driven convection), the heat and mass transfer, and the chemical reactions. For example, large thermal gradients can generate buoyancy-driven secondary flows and/or thermal diffusion effects that lead to spatial and/or temporal variations in film deposition rates and composition. Typically, metal organic chemical vapor deposition (MOCVD) processes are operated in a pressure range from 20 to 760 Torr, where transport processes can strongly influence the supply of reactants to the growing film, the growth rate, and the uniformity of deposition.

The rotating disk reactor (RDR) has the potential to achieve the uniform transport properties that are characteristic of an infinite rotating disk in an infinite medium. Previous studies by Evans and Greif [1]-[2], Patnaik et al. [3], and Fotiadis et al. [4] have examined these effects for a single component gas in nonisothermal RDR's. Palmateer et al. [5] noted convective instabilities in an experimental study of isothermal gas mixing in a stagnation flow reactor. Recent studies by Winters et al. [6]-[7] showed that large concentration gradients also generate buoyancy-driven secondary flows. All the previous studies considered reactors with large inlet to disk separation distances ($A=\overline{\mathrm{H}}/\overline{r}_d > 2$; cf. Fig. 1). Recent interest in combined rotating disk/stagnation flow reactors has focused on smaller values of A. The present study addresses geometrical aspects of the basic rotating disk/stagnation flow CVD reactor with regard to flow stability and heat transfer uniformity.

The axisymmetric, circumferentially uniform Navier-Stokes and energy equations are solved for the H_2 carrier gas in the vertical RDR geometry shown in Figure 1. The solutions are normalized with the infinite rotating disk/stagnation flow (Evans and Greif [8], Coltrin et al. [9]) similarity solution results in which an infinite rotating disk is separated by a distance $\overline{\mathrm{H}}$ from an infinite non-rotating disk through which gas flows toward the rotating disk. To further elucidate the effects of $\overline{\mathrm{H}}$ on the heat transfer from the disk and on the flow patterns between the disk and the gas inlet, results from the 1D similarity solution for the rotating/stagnation flow are presented as a function of SP and Re_ω. The trends predicted from the similarity solution are then verified in the 2D solutions where the effects of buoyancy and finite radial geometry are included. The 2D solutions are obtained for axial aspect ratios A of 0.54 and 2.16, radial aspect ratios $\overline{r}_o/\overline{r}_d$ of 1.1, 1.2, and 1.4, flow parameter values $\mathrm{SP}=|\overline{u}_{\mathrm{in}}|/\sqrt{\overline{\nu}_{\mathrm{in}}\overline{\omega}}$ from 0.23 to 1.38, and disk Reynolds numbers Re_ω from 76 to 456.

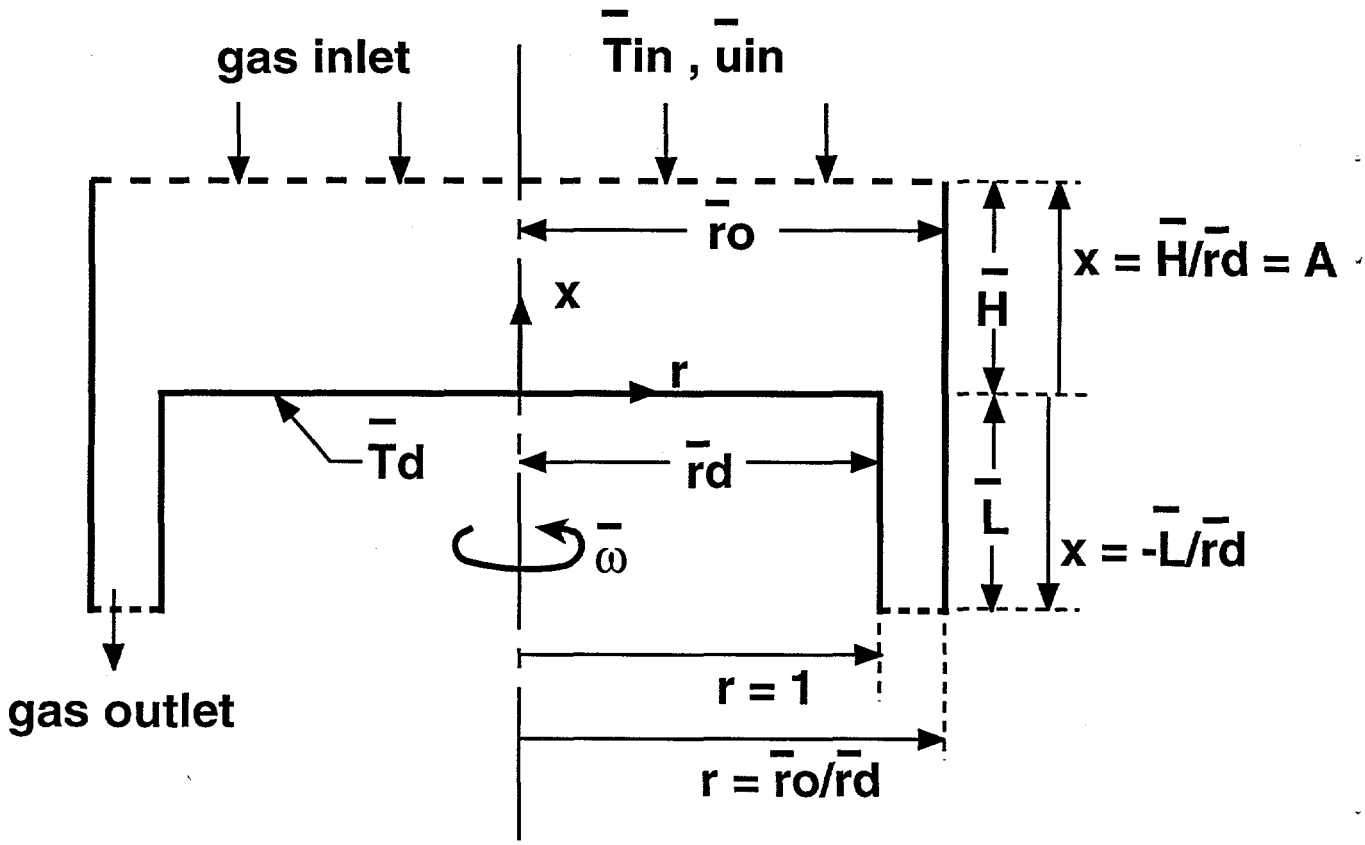

Figure 1: Geometry and coordinate system.

3 Problem definition

The steady dimensionless equations for mass, momentum, and energy conservation are given (in cylindrical coordinates) by:

$$\frac{1}{r}\frac{\partial\,(r\rho v)}{\partial r}+\frac{\partial\,(\rho u)}{\partial x}=0 \tag{1}$$

$$\frac{1}{r}\frac{\partial}{\partial r}\left(r\rho vu\;-\;\frac{r\mu}{\mathrm{Re}_\omega}\frac{\partial u}{\partial r}\right)+\frac{\partial}{\partial x}\left(\rho uu-\mu\frac{\partial u}{\partial x}\right)=-\frac{\partial p_m}{\partial x}+\frac{\mathrm{Gr}}{{\mathrm{Re}_\omega}^{3/2}}\frac{(1-\rho)}{(1-\rho_d)}$$
$$+\;\frac{1}{r}\frac{\partial}{\partial r}\left(r\mu\frac{\partial v}{\partial x}\right)+\frac{\partial}{\partial x}\left\{\mu\frac{\partial u}{\partial x}-\frac{2\mu}{3}\left[\frac{1}{r}\frac{\partial(rv)}{\partial r}+\frac{\partial u}{\partial x}\right]\right\} \tag{2}$$

$$\frac{1}{r}\frac{\partial}{\partial r}\left(r\rho vv\;-\;\frac{r\mu}{\mathrm{Re}_\omega}\frac{\partial v}{\partial r}\right)+\frac{\partial}{\partial x}\left(\rho uv-\mu\frac{\partial v}{\partial x}\right)=-\frac{1}{\mathrm{Re}_\omega}\frac{\partial p_m}{\partial r}+r\rho f^2$$
$$+\;\frac{1}{\mathrm{Re}_\omega}\frac{1}{r}\frac{\partial}{\partial r}\left\{r\mu\left[\frac{\partial v}{\partial r}-\frac{2}{3}\left(\frac{1}{r}\frac{\partial(rv)}{\partial r}+\frac{\partial u}{\partial x}\right)\right]\right\}$$

$$- \frac{1}{\mathrm{Re}_\omega}\frac{\mu}{r}\left\{\frac{2v}{r} - \frac{2}{3}\left[\frac{1}{r}\frac{\partial(rv)}{\partial r} + \frac{\partial u}{\partial x}\right]\right\} + \frac{1}{\mathrm{Re}_\omega}\frac{\partial}{\partial x}\left(\mu\frac{\partial u}{\partial r}\right) \qquad (3)$$

$$\frac{1}{r}\frac{\partial}{\partial r}\left(r\rho v f - \frac{r\mu}{\mathrm{Re}_\omega}\frac{\partial f}{\partial r}\right) + \frac{\partial}{\partial x}\left(\rho u f - \mu\frac{\partial f}{\partial x}\right) = -\frac{2\rho v f}{r} + \frac{1}{\mathrm{Re}_\omega}\frac{2\mu}{r}\frac{\partial f}{\partial r} \qquad (4)$$

$$\frac{1}{r}\frac{\partial}{\partial r}\left(r\rho v\Theta - \frac{r}{\mathrm{Re}_\omega \mathrm{Pr}}\frac{k}{c_p}\frac{\partial \Theta}{\partial r}\right) + \frac{\partial}{\partial x}\left(\rho u\Theta - \frac{1}{\mathrm{Pr}}\frac{k}{c_p}\frac{\partial \Theta}{\partial x}\right) =$$

$$\frac{1}{\mathrm{Pr}}\frac{k}{{c_p}^2}\left(\frac{1}{\mathrm{Re}_\omega}\frac{\partial \Theta}{\partial r}\frac{\partial c_p}{\partial r} + \frac{\partial \Theta}{\partial x}\frac{\partial c_p}{\partial x}\right) \qquad (5)$$

where $f \equiv w/r$ in equation (4), and the dimensionless parameters in equations (1)-(5) are: $\mathrm{Gr} = \overline{g}\,(\overline{\rho}_{\mathrm{in}} - \overline{\rho}_d)\overline{r}_d{}^3/(\overline{\rho}_{\mathrm{in}}\overline{\nu}_{\mathrm{in}}^2)$, $\mathrm{Re}_\omega = \overline{r}_d{}^2\overline{\omega}/\overline{\nu}_{\mathrm{in}}$, and $\mathrm{Pr} = \overline{\nu}_{\mathrm{in}}/\overline{\alpha}_{\mathrm{in}}$; the fluid properties have been normalized with their respective values at the inlet of the reactor. The usual scaling (Evans and Greif [1]; White [10]) for a rotating disk has been used: $\sqrt{\overline{\omega}\,\overline{\nu}_{\mathrm{in}}}$ for the axial component of velocity, $\overline{r}_d\overline{\omega}$ for the radial and circumferential components of velocity, $\sqrt{\overline{\nu}_{\mathrm{in}}/\overline{\omega}}$ for the axial coordinate and $\overline{r}_d$ for the radial coordinate, where symbols with overbars represent dimensional quantities. The boundary conditions are:

$x = 0$	$0 \le r \le 1$	$u = v = 0, \quad f = \Theta = 1$
$r = \overline{r}_o/\overline{r}_d$	$-\overline{L}/\overline{r}_d \le x \le A$	$u = v = f = \Theta = 0$
$r = 1$	$-\overline{L}/\overline{r}_d \le x \le 0$	$u = v = f = \partial\Theta/\partial r = 0$
$r = 0$	$0 \le x \le A$	$\partial u/\partial r = \partial f/\partial r = \partial\Theta/\partial r = v = 0$
$x = A$	$0 \le r \le \overline{r}_o/\overline{r}_d$	$v = f = \Theta = 0,$
		$u = -\mathrm{Re}_{\mathrm{in}}/(A\sqrt{\mathrm{Re}_\omega}) = \overline{u}_{\mathrm{in}}/\sqrt{\overline{\omega}\,\overline{\nu}_{\mathrm{in}}} = -\mathrm{SP}$
$x = -\overline{L}/\overline{r}_d$	$1 \le r \le \overline{r}_o/\overline{r}_d$	$\partial u/\partial x = \partial v/\partial x = \partial f/\partial x = \partial\Theta/\partial x = 0.$

4 Numerical Solution

4.1 Methodology

The nonlinear 1D similarity solution equations [8] are solved using Newton's method in a boundary value problem code (Grcar [11]) with solution adaptive grid refinement (see Coltrin et al. [12]). Convergence of the results was checked by varying the absolute and relative error tolerances from 10^{-8} to 10^{-9} and from 10^{-5} to 10^{-6}, respectively. Computational times for the 1D solution were typically 1-4 sec on a SGI/R8000 computer.

The 2D conservation equations (1)-(5) are integrated over control volumes and discretized using either central differences for all remaining derivatives or the hybrid

differencing scheme (Patankar [13]). The SIMPLER method is used to determine the pressure, p_m. A sequential line by line relaxation scheme is used to solve the discretized equations and boundary conditions discussed above. An iterative method was used to solve the coupled, nonlinear set of equations. Underrelaxation factors (typical values ranged from 0.3 to 0.5) were used for the momentum and energy conservation equations to avoid numerical instabilities; no underrelaxation was applied to the pressure equation. Iterations were continued until changes in heat flux at the surface of the rotating disk were negligible. The axial component of velocity was determined to be the quantity that was the most sensitive indicator of convergence. Typically, 10000-15000 iterations were required to obtain convergence; computational times were 4-6 and 3-5 hours on a HP 735/99 and on a SGI/R8000, respectively.

4.2 Grid Sensitivity

The 1D results were checked by varying gradient and curvature adaptive grid control parameters in SPIN [12] from 0.03 to 0.1. Typically, 100 grids (obtained with grid control parameter values of about 0.07) were required to obtain grid-independent results.

The 2D results were obtained on a nonuniform grid of 30 by 70 control volumes in the x and r directions, respectively, with finer grid spacings near the rotating disk ($x = 0$) and the symmetry axis ($r = 0$) of the reactor. Calculations were also made on a nonuniform x,r grid of 60 by 80 control volumes. Results for the baseline case (shown in Figs. 5a,b) differed by less than 1% for the two grid distributions. Furthermore, the excellent agreement between the 1D and 2D velocity and temperature profiles across the boundary layer for the baseline case discussed below shows the adequacy of the 2D grid distribution (cf. Fig. 5b at $r = 0$).

5 Results and Discussion

The basic flow in the reactor is a combination of a high-speed rotating disk flow and a stagnation flow. In an ideal rotating disk flow (infinite disk in an infinite medium), the gas velocity normal to the disk approaches an asymptotic value at the outer edge of the boundary layer. This value depends on the properties of the fluid as well as the rotation speed of the disk, and for gases and temperatures typical of MOCVD, the dimensionless asymptotic velocity, $\overline{u}_{\text{asym}}/\sqrt{\overline{\omega}\ \overline{\nu}_{\text{in}}}$, varies from 0.7 to 0.9, approximately ([1], [10]). The similarity solution referred to earlier allows a uniform gas velocity normal to the disk to be specified (in dimensionless form, SP$=|\overline{u}_{\text{in}}|/\sqrt{\overline{\omega}\ \overline{\nu}_{\text{in}}}$)

at a distance, $\overline{H}$, from the disk. In an actual reactor the finite dimensions of the reactor and buoyancy are additional parameters that can affect the uniformity of the boundary layers. For instance, if the distance between the gas inlet and the disk is smaller than the thicknesses of the disk boundary layers (thermal and momentum), then the flow may deviate from the uniform flow and heat transfer characteristics of the similarity solution. In situations where buoyancy may be important, an inlet velocity that is larger than the asymptotic value for the infinite rotating disk should reduce boundary layer thicknesses and have a potentially stabilizing effect on the flow. On the other hand, reducing the gas velocity to below the asymptotic value for an infinite rotating disk has been shown to result in recirculating flow ([1], [2]) for reactors with values of A>2. For all 2D results shown the buoyancy effect is small (the mixed convection parameter, $Gr/Re_\omega{}^{3/2}$, is less than 2.5) except for the two cases in Fig. 7 with Re_ω =76 ($Gr/Re_\omega{}^{3/2}$ = 12.2); in those two cases the ratio of the inlet velocity to the rotating disk asymptotic drawing velocity is large (SP=1.3).

In the results presented here the effects of small to moderate values of A (0.54 and 2.16) on flow and heat transfer uniformity are determined as functions of SP, Re_ω, and $\overline{r}_o/\overline{r}_d$ (1.1, 1.2 and 1.4). The inlet velocity is varied from 5 to 40 cm/s (Re_{in} from 2.77 to 11.09 for A=0.54; from 11.08 to 44.36 for A=2.16) and the rotation rate is varied from 50 to 1200 rpm (Re_ω from 19 to 456), yielding values of SP that vary from 0.23 to 8.96. Thus, the inlet velocity is varied from values that are significantly less than to significantly greater than the asymptotic value for an infinite rotating disk (from "starving" the disk to "forcing" it). In all cases studied (both 1D and 2D), the gas is H_2, $\overline{T}_{in}$=50 C, and $\overline{T}_d$=800 C. The heat transfer is presented in terms of the dimensionless Nusselt number, defined as:

$$Nu = \frac{\overline{q}|_{\overline{x}=0}}{(\overline{T}_d - \overline{T}_{in})} \frac{\sqrt{\overline{\nu}_{in}/\overline{\omega}}}{\overline{k}_{in}} = -\left(k\frac{\partial\Theta}{\partial x}\right)\Big|_{x=0} \qquad (6)$$

where $\overline{q}|_{\overline{x}=0} = -(\overline{k}\,\partial\overline{T}/\partial\overline{x})|_{\overline{x}=0}$.

5.1 Similarity solution results

The effects of reactor height $\overline{H}$ on the flow and heat transfer for different flow rates and spin rates were studied first with the 1D computer code SPIN [12] that incorporates the similarity transformation for the rotating/stagnation flow between two infinite disks; one disk is rotating and the other (through which gas flows) is stationary. The results of the similarity solution provide valuable trends and aid in interpreting the more complex results of the 2D calculations presented later. Although the similarity solutions are for infinite radial extent, values of $\overline{r}_d$ =3.7 cm

and $\overline{r}_o$=4.4 cm are used here in the calculation of the dimensionless parameters A, SP, and Re_ω to facilitate comparison with the 2D results. In Figs. 2 and 3 below, Nu_{1D} and SP are normalized with their values at the baseline conditions of ϵ=2.32, $|\overline{u}_{in}|$=20 cm/s, $\overline{\omega}$=600 rpm, P=250 Torr, and A=0.54 (SP_{ref} = 1.3, $\mathrm{Nu}_{1D_{ref}}$ = 0.354).

The similarity solution results for the variation of the one-dimensional Nusselt number Nu_{1D} with SP for two values of the axial aspect ratio (A=0.54 and 2.16) and for Re_ω=228 (600 RPM) are shown in Fig. 2 (note that for fixed gas properties at the inlet and fixed disk rotation rate, variations in SP correspond to variations in the inlet gas velocity). Figure 2 shows that Nu_{1D} increases approximately linearly with SP for both values of A; however, the variation of Nu_{1D} with SP is much larger for the smaller value of A.

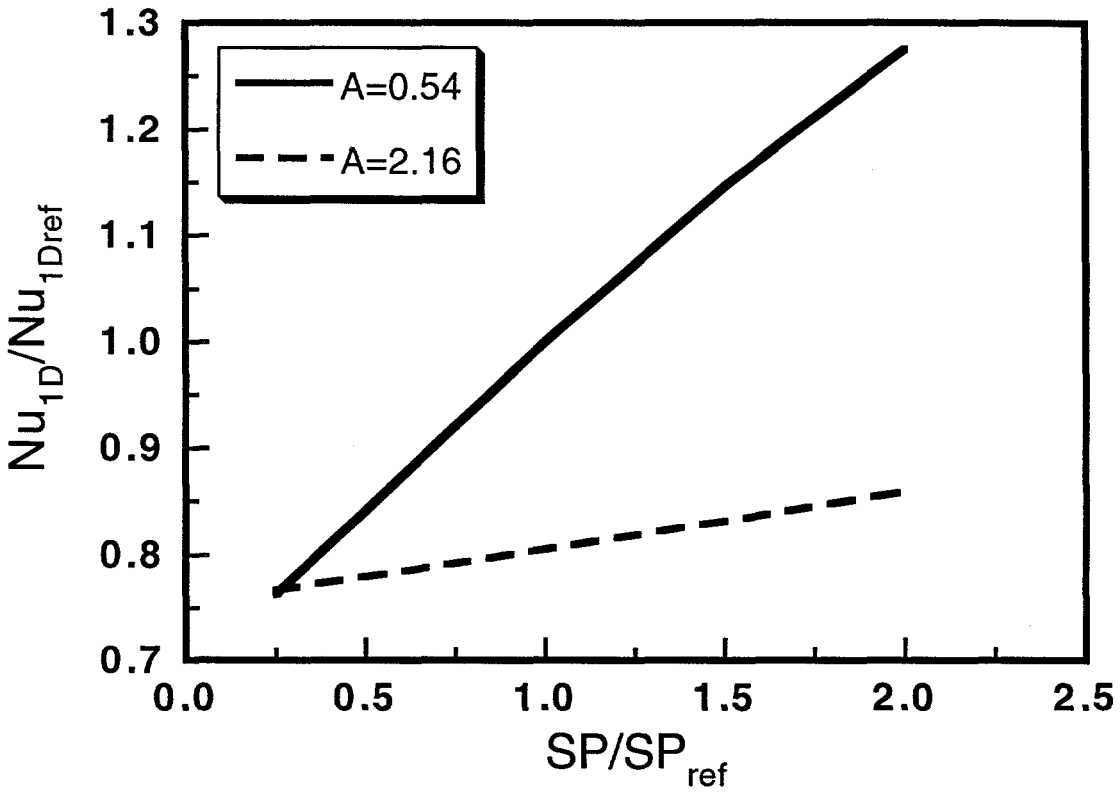

Figure 2: Variation of disk heat transfer (Nu_{1D}) with inlet gas velocity (SP) from the 1D similarity solution for two gas inlet to rotating disk spacings (A=0.54 and 2.16) and for a fixed disk rotation rate (Re_ω=228). The normalization, $\mathrm{Nu}_{1D_{ref}}$, is for A=0.54.

For both values of A and for fixed inlet velocity ($|\overline{u}_{in}|$=20 cm/s), Nu_{1D} is shown in Fig. 3a to decrease with increasing Re_ω and to reach an asymptotic value that is equal to the Nusselt number for an infinite rotating disk at $\mathrm{Re}_\omega \approx 450$.

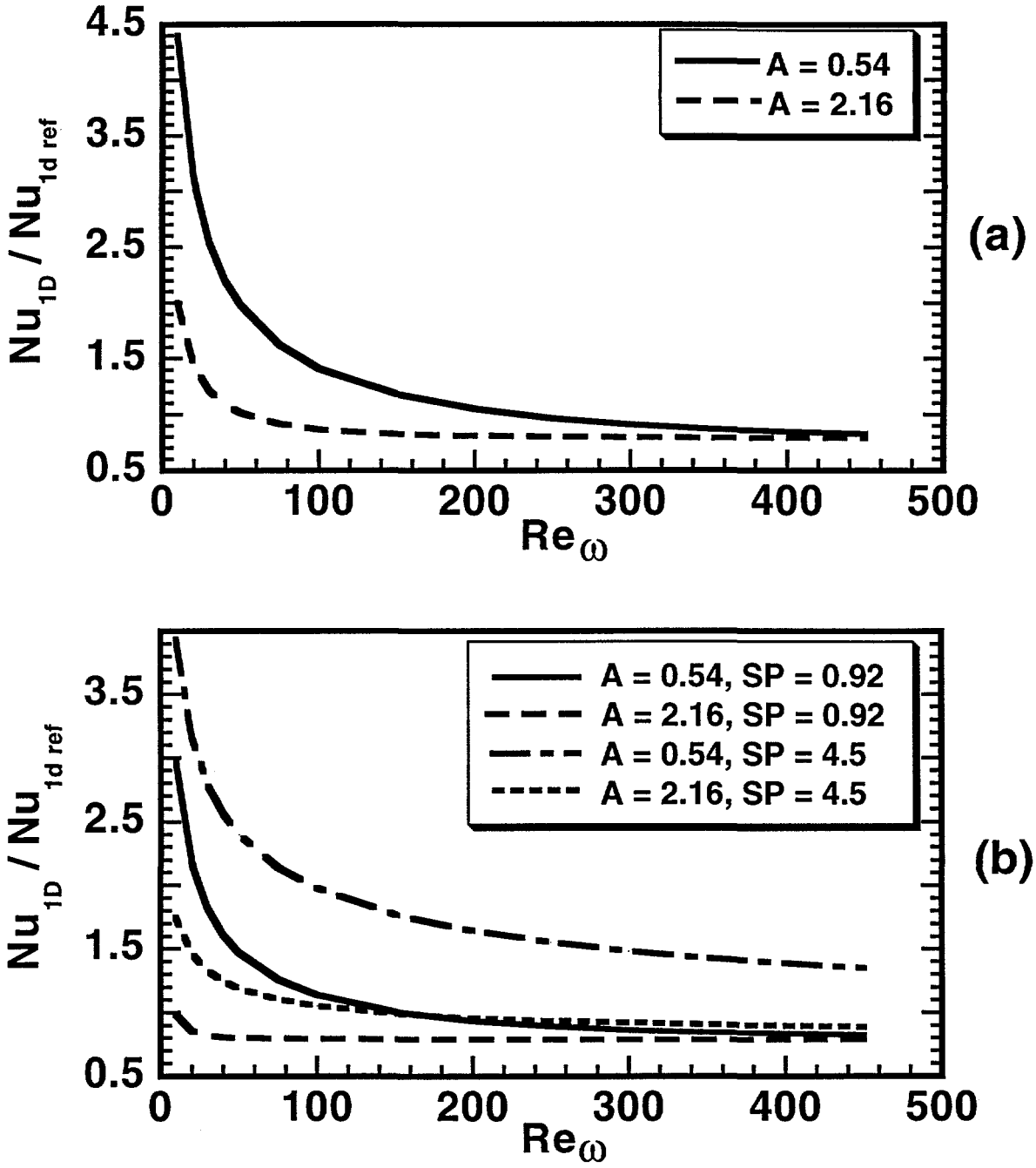

Figure 3: (a) Variation of disk heat transfer (Nu_{1D}) with disk rotation rate (Re_ω) from the 1D similarity solution for two gas inlet to rotating disk spacings (A=0.54 and 2.16) and for a fixed inlet gas velocity ($|\overline{u}_{in}|$=20 cm/s). The normalization, $Nu_{1D_{ref}}$, is for A=0.54 and Re_ω=228; (b) Variation of disk heat transfer (Nu_{1D}) with disk rotation rate (Re_ω) from the 1D similarity solution for two gas inlet to rotating disk spacings (A=0.54 and 2.16) and for two values of SP (0.92 and 4.5). The normalization, $Nu_{1D_{ref}}$, is for A=0.54, Re_ω=228, and SP=1.3.

The variation of Nu_{1D} with Re_ω is larger for the smaller spacing (A=0.54). Note that SP increases from 0.92 to 4.5 in Fig. 3a as Re_ω decreases from 456 to 19 ($|\overline{u}_{in}|$ is fixed at 20 cm/s). The variation of Nu_{1D} with Re_ω for A=0.54 and 2.16 at two values of SP (0.92 and 4.5) is shown in Fig. 3b; at the larger spacing (A=2.16) and for the smaller value of SP (SP=0.92), Nu_{1D} is approximately constant and equal to the value for the infinite rotating disk. As noted in Fig. 3a for fixed inlet velocity, the variation of Nu_{1D} with Re_ω is larger at the smaller spacing (A=0.54) for both values of SP shown in Fig. 3b. Over the range of Re_ω studied, Nu_{1D} for the case with A=0.54 and SP=4.5 is significantly larger than the asymptotic value for an infinite rotating disk. The effect of SP on Nu_{1D} is larger for A=0.54 than it is for A=2.16 for all values of Re_ω studied.

The effects of spacing (A=0.54 and 2.16) and SP (0.23 and 0.92) on the axial profiles (between the inlet and the rotating disk) of the radial component of velocity are shown in Fig. 4 from the 1D similarity solution for $Re_\omega = 456$ ($\overline{\omega}$= 1200 rpm), where A=0.54 corresponds to $\overline{H}$=2 cm and A=2.16 corresponds to $\overline{H}$=8 cm.

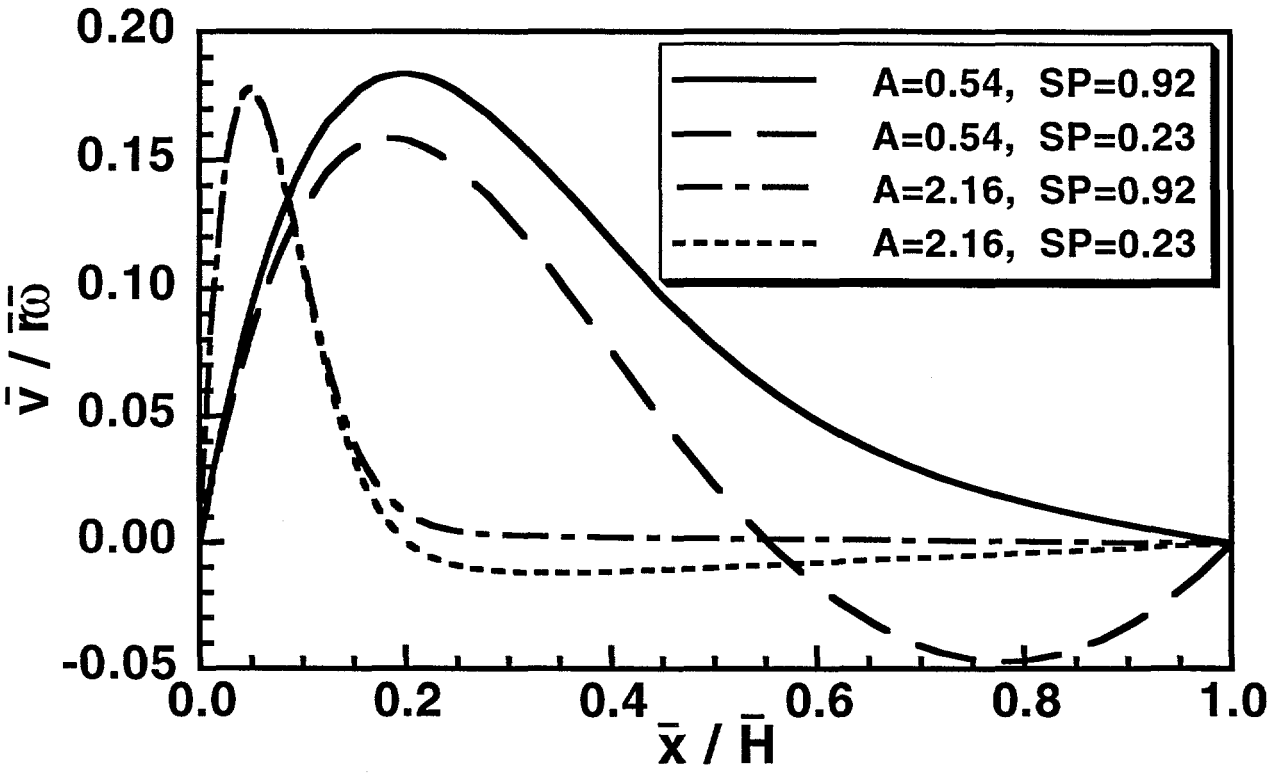

Figure 4: Axial variation of radial component of velocity ($v = \overline{v}/(\overline{r}\overline{\omega})$) from the 1D similarity solution for two gas inlet to rotating disk spacings (A=0.54 and 2.16) and for two values of SP (0.23 and 0.92) for Re_ω=456 ($\overline{\omega}$=1200 rpm).

For the smaller value of SP=0.23, the radial velocity is negative over a significant

fraction of the distance between the inlet and the disk (starting from the inlet and extending toward the disk) for both values of A. For the larger value of SP=0.92, the radial component of velocity is positive everywhere between the inlet and the rotating disk for both values of A. As noted above for the heat transfer, the effect of SP on the radial component of velocity is greater (there is a larger negative radial velocity component) at the smaller spacing.

In summary, the similarity solution results show large effects of SP (inlet velocity for fixed disk rotation rate and fixed inlet gas properties) and Re_ω (disk rotation rate for fixed disk radius and fixed inlet gas properties) on Nu_{1D} for small A. For large A the effects of SP and Re_ω on Nu_{1D} are much smaller. Similarly, for the flow, the axial profile of the radial component of velocity is shown to be affected significantly by changes to SP at small A; a smaller effect of SP is noted at larger values of A.

5.2 2D results

The radial variation of the dimensionless local heat transfer $\mathrm{Nu}_{2D}/\mathrm{Nu}_{1D}$ from the rotating disk to the gas flow is shown in Fig. 5a for the baseline conditions: SP=1.3, Re_ω =228, A=0.54, and $\overline{r}_o/\overline{r}_d$ =1.2. Over the inner half of the disk (r<0.5) the local heat transfer is uniform and identical to the 1D result; for r>0.5, the increase in Nu_{2D} is the result of edge effects due to the flow acceleration and the change of flow direction from radial near the disk to axial in the annular outflow region (x<0, cf. Fig. 1). The axial (x) profiles of T and u from the 2D and the similarity (1D) solutions are compared at three radial locations (r=0, 0.66, 1.0) for the baseline conditions in Fig. 5b; there is excellent agreement for $r \leq 0.66$. For the conditions of Figs. 5a,b the inlet velocity exceeds the asymptotic ideal rotating disk speed by 42% ($|\overline{u}_{\mathrm{in}}|$=20 cm/s, $\overline{u}_{\mathrm{ideal}}$=14 cm/s; $\mathrm{SP}=\mathrm{Re}_{\mathrm{in}}/(A\sqrt{\mathrm{Re}_\omega}) = |\overline{u}_{\mathrm{in}}|/\sqrt{\omega\,\overline{r}_{\mathrm{in}}} = 1.3$).

The effects of (a) spacing between the gas inlet and the rotating disk, (b) inlet velocity, and (c) disk rotation on the disk heat transfer are shown in Figs. 6 and 7 (the normalizing factor Nu_{1D} varies for each curve, depending on SP, Re_ω, and A). Figure 6 shows the variation of Nu_{2D} with radial position for Re_ω =456 (1200 RPM), for SP=0.46 and 1.38, and for A=0.54 and 2.16. For A=2.16, the radial variation of Nu_{2D} is also shown for the case where the inlet velocity matches the asymptotic value for an infinite rotating disk, SP=0.81. At the smaller spacing (A=0.54) Nu_{2D} is uniform to within 1% for r<0.5 for both values of SP; for r>0.5, there is greater nonuniformity for the larger value of SP. At the larger spacing (A=2.16) the radial variation of Nu_{2D} is also larger for the larger value of SP (SP=1.38); for the smaller value of SP (SP=0.46), Nu_{2D} decreases from $r=0$ to $r\approx$0.7 and then increases for r>0.7; for the case where the inlet velocity matches the asymptotic value for the

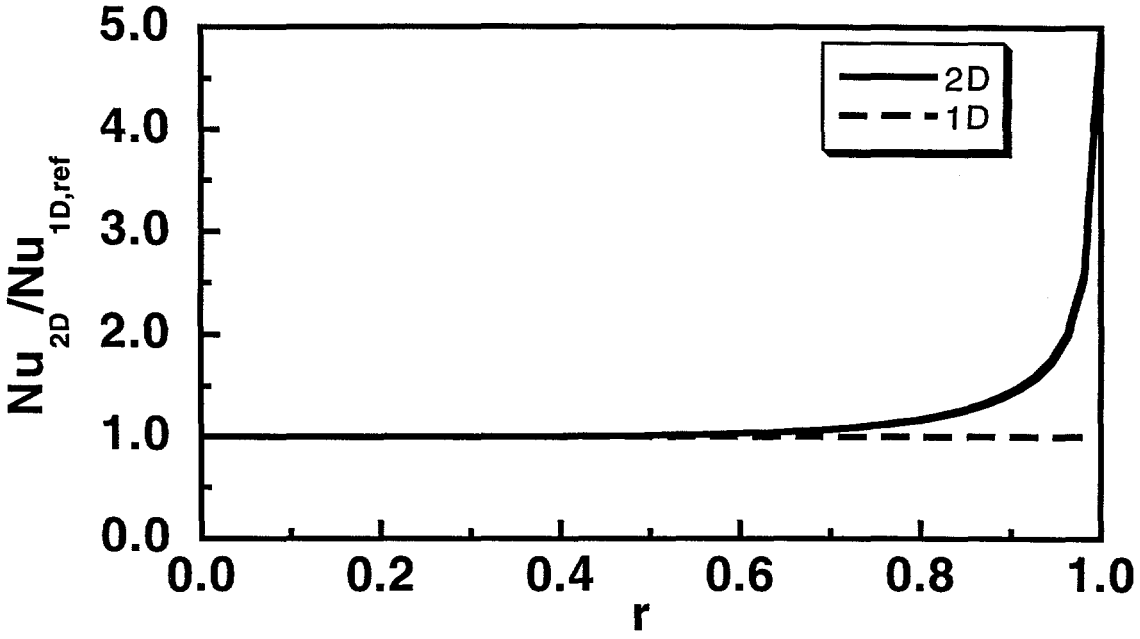

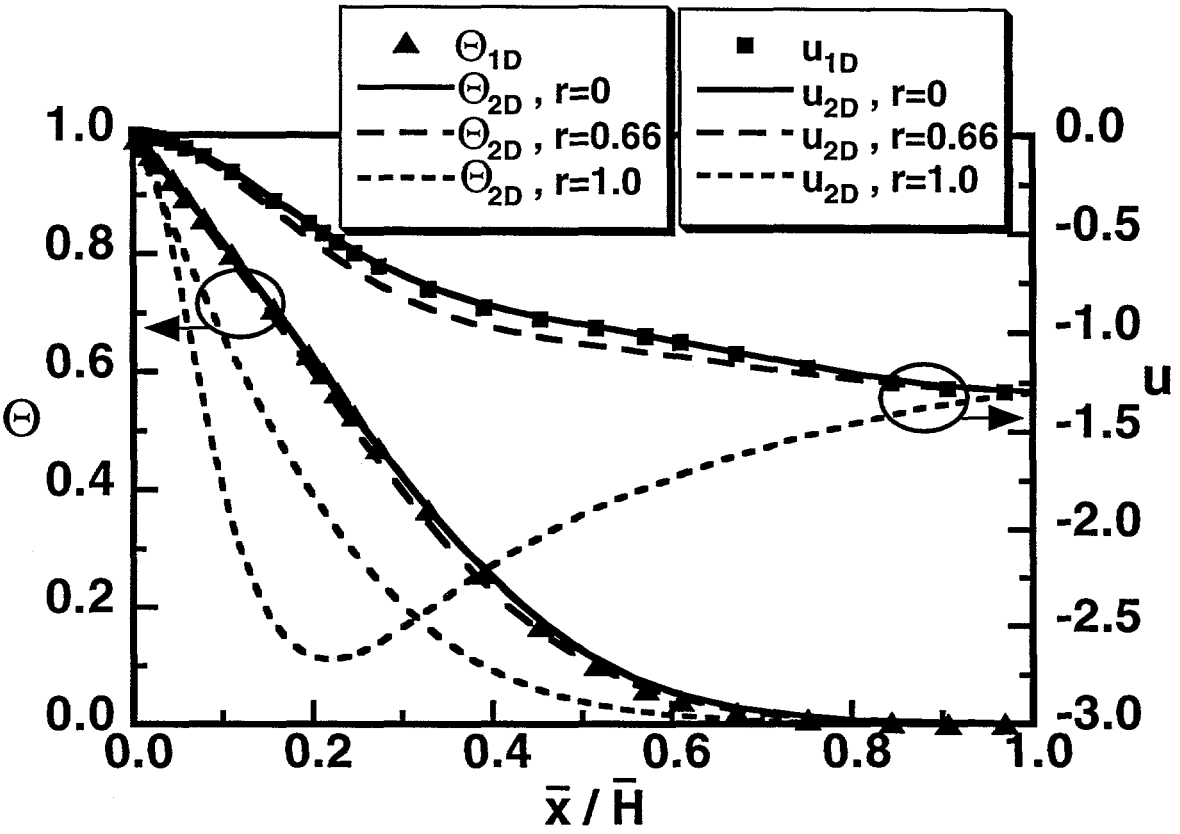

Figure 5: (a) Radial variation of disk heat transfer from the 2D solution (Nu_{2D}) for the baseline conditions: SP=1.3, Re_ω=228, A=0.54, and $\bar{r}_o/\bar{r}_d$ =1.2; comparison with the 1D similarity solution; (b) Axial profiles of temperature (Θ) and axial component of velocity (u) from the 2D solution at three radial positions (r=0, 0.66, and 1.0) for the baseline conditions: SP=1.3, Re_ω=228, A=0.54, and $\bar{r}_o/\bar{r}_d$ =1.2; comparison with the 1D similarity solution.

infinite rotating disk (SP=0.81), Nu_{2D} is uniform to within 1.3% for $r<0.5$. Figure 6 shows that the inlet velocity (SP) has a larger effect on the radial variation of the heat transfer from the rotating disk for larger values of A (at the larger value of A, radial uniformity is improved greatly by matching the inlet velocity to the asymptotic velocity of an infinite rotating disk); for both values of A, Nu_{2D} increases significantly with r for the higher value (1.38) of SP.

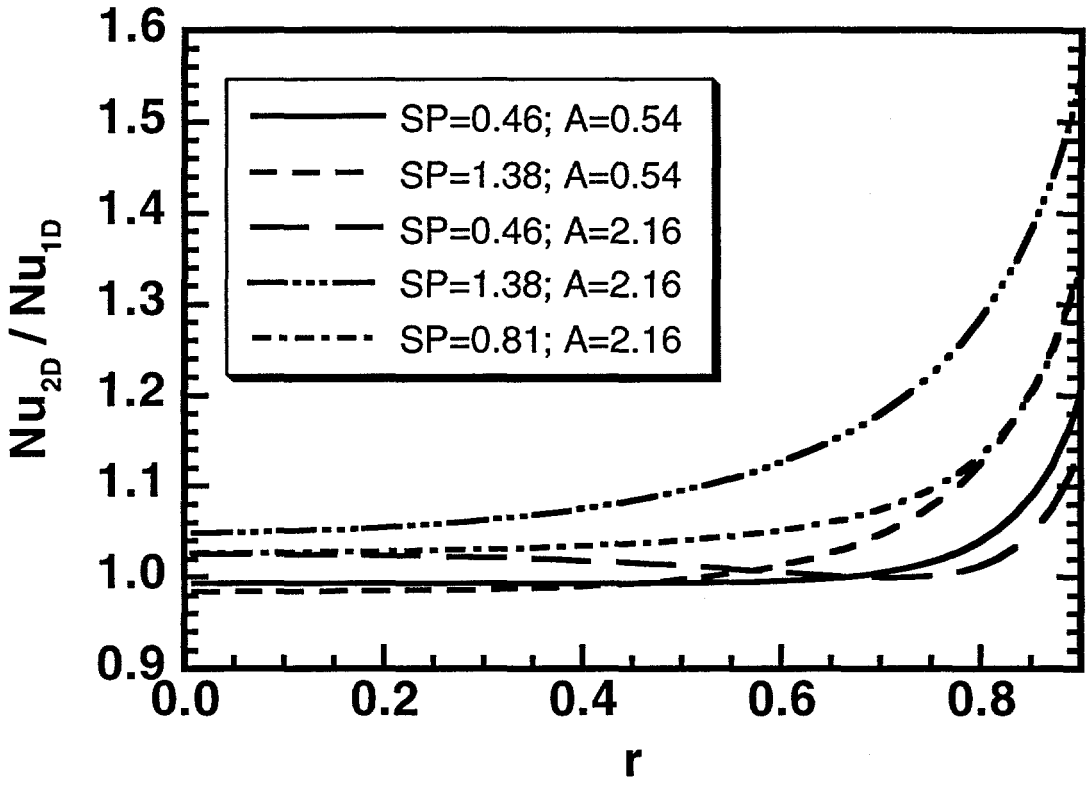

Figure 6: Radial variation of disk heat transfer from the 2D solution (Nu_{2D}) for two gas inlet to rotating disk spacings (A=0.54 and 2.16), for Re_ω =456, $\overline{r}_o/\overline{r}_d$ =1.2, and for two values of SP (0.46 and 1.38); also shown is the result for A=2.16 when the inlet velocity is matched to the infinite rotating disk asymptotic drawing velocity (SP=0.81).

Figure 7 shows the variation of Nu_{2D} with radial position for SP=1.3, for Re_ω =76 and 228, and for A=0.54 and 2.16. For both values of A, there is greater radial variation in Nu_{2D} at the smaller value of Re_ω ; the largest radial variation in Nu_{2D} occurs for the combination Re_ω =76 (smaller rotation rate) and A=2.16 (larger spacing).

The effect of A on the flow pattern and the temperature field is shown in Figs. 8a-d for $Re_\omega = 456$ and SP=0.23. Note that for this value of SP, the inlet velocity is significantly less than what is required by an infinite rotating disk; this results

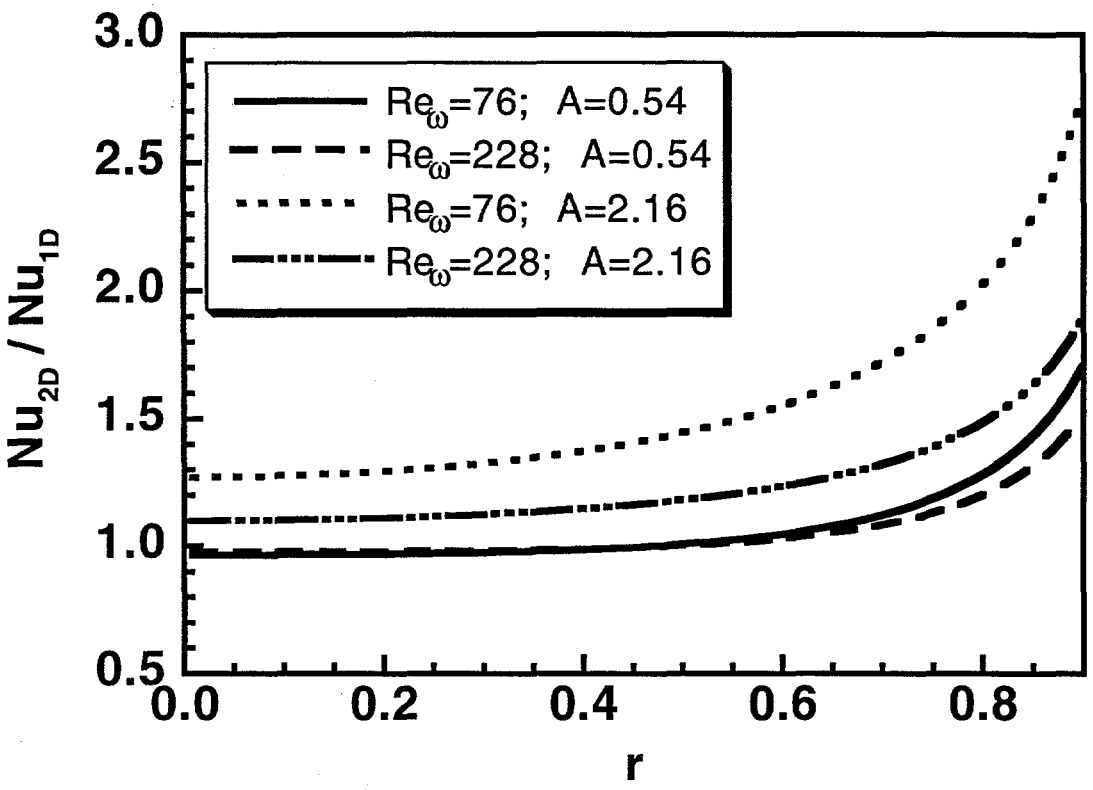

Figure 7: Radial variation of disk heat transfer from the 2D solution (Nu_{2D}) for two gas inlet to rotating disk spacings (A=0.54 and 2.16), for SP=1.3, $\overline{r}_o/\overline{r}_d$ =1.2, and for two values of Re_ω (76 and 228).

in "starving" the rotating disk. For A=0.54, the heat transfer is uniform and in excellent agreement with the 1D result (not shown) whereas for A=2.16, larger heat transfer occurs near the centerline of the disk (seen in the temperature field isotherms in Figs. 8a,c). The flow recirculates for both values of A (cf. Figs. 8b,d). However, for the smaller value of A the recirculation region is smaller (cf. Fig. 8d) due to the smaller gap between the inlet and the rotating disk. Note that the radial velocity component shown in Fig. 4 for this small value of SP and both values of A is negative over a part of the region between the inlet and the rotating disk. From the one-dimensional analysis (Fig. 4) the recirculation region shown in the two-dimensional results of Figs. 8b,d is expected.

Figs. 8a,c show the isotherms for these two values of A; in Fig. 8c, the thermal boundary layer extends all the way to the gas inlet and the isotherms are parallel to the disk surface. The larger height and larger flow recirculation cell of Fig. 8b results in isotherms that are not parallel to the disk (Fig. 8a), leading to the nonuniform heat transfer (not shown) for A=2.16.

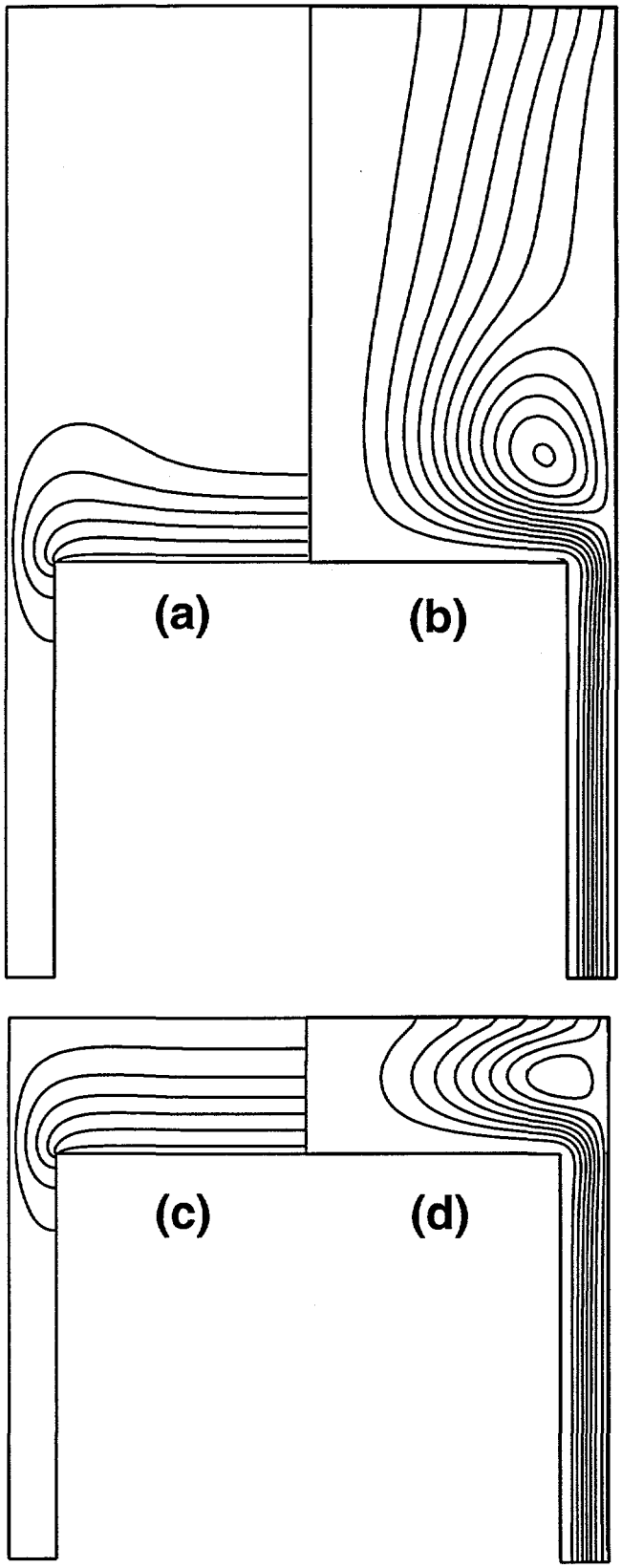

Figure 8: Temperature and velocity fields (isotherms and streamlines) from the 2D solution for two gas inlet to rotating disk spacings (A=0.54 and 2.16), for SP=0.23 and Re_ω =456; (a) isotherms for A=2.16: min. 300 K, max. 1100 K, inc. 120 K; (b) streamlines for A=2.16: min. 0.001 cm^2/s, max. 0.012 cm^2/s, inc. 0.001 cm^2/s; (c) isotherms for A=0.54: min. 300 K, max. 1100 K, inc. 120 K; (d) streamlines for A=0.54: min. 0.001 cm^2/s, max. 0.008 cm^2/s, inc. 0.001 cm^2/s.

The radial aspect ratio, $\overline{r}_o/\overline{r}_d$, was varied from 1.1 to 1.4 for the conditions A=0.54, Re_ω =456, and SP=0.23 (not shown) to determine its effect on the recirculation shown in Fig. 8d and on the radial uniformity of Nu_{2D}. The heat transfer was slightly more uniform for larger $\overline{r}_o/\overline{r}_d$. For all three values of $\overline{r}_o/\overline{r}_d$, Nu_{2D} varied by less than 2% for r<0.8; at r=0.9, Nu_{2D} was 8% larger than the 1D result for $\overline{r}_o/\overline{r}_d$ =1.4, increasing to 24% larger for $\overline{r}_o/\overline{r}_d$ =1.1. For $\overline{r}_o/\overline{r}_d$ =1.1, the gas recirculation region above the rotating disk was similar to that shown in Fig. 8d; for $\overline{r}_o/\overline{r}_d$ =1.4, the recirculation region was reduced somewhat. However, for all three values of $\overline{r}_o/\overline{r}_d$ there was a significant radial inflow (toward $r=0$) for x>0.5. This radial inflow is consistent with the similarity solution results shown in Fig. 4 for the same conditions.

6 Conclusions

The flow and heat transfer of hydrogen gas in a vertical high-speed rotating disk/stagnation flow chemical vapor deposition (CVD) reactor has been studied numerically with particular emphasis on the effects of the spacing, $\overline{\mathrm{H}}$, between the gas inlet and the rotating disk. Both one-dimensional and two-dimensional analyses were used to determine the effects of operating parameters and reactor geometry on the flow and heat transfer. The 1D results show that the dimensionless heat transfer from the rotating disk, Nu_{1D} , depends on SP and Re_ω to a much greater extent at smaller spacings (axial aspect ratio A=$\overline{\mathrm{H}}/\overline{r}_d$ =0.54) than at larger spacings (A=2.16). For either fixed inlet velocity ($|\overline{u}_{\mathrm{in}}|$=20 cm/s) or fixed SP (SP=0.92 and 4.5) and for both spacings studied (A=0.54 and 2.16), Nu_{1D} approaches the value for an infinite rotating disk for $\mathrm{Re}_\omega \approx 450$, except for the case at the larger SP (4.5) and the smaller spacing (A=0.54) where Nu_{1D} is significantly larger. The similarity solution results show that for small SP (0.23) there is a significant flow toward $r=0$ (the radial component of velocity is negative) which is larger for the smaller value of A.

The 2D results show that the effect of inlet velocity (SP) on the radial variation of the disk heat transfer (Nu_{2D}) is greater for larger values of A; for both values of A there is greater radial variation of Nu_{2D} at the larger value of SP. At the larger A, the radial uniformity of Nu_{2D} is improved significantly when the inlet velocity matches the asymptotic value for an infinite rotating disk. For both values of A there is gas recirculation above the rotating disk when the disk is "starved" significantly (SP=0.23, Re_ω =456). This result is expected based on the negative values of the radial component of velocity from the 1D similarity solution results at the same operating conditions. For the conditions SP=0.23 and Re_ω =456, the

thermal boundary layer extends to the gas inlet for A=0.54 and Nu_{2D} is uniform; for A=2.16, Nu_{2D} varies by more than 10% for $0 \leq r \leq 0.8$. The uniformity of Nu_{2D} and the recirculation of the gas above the disk were affected by only a small amount when the radial aspect ratio, $\overline{r}_o/\overline{r}_d$, was varied by approximately 30% (from 1.1 to 1.4) for the conditions SP=0.23, A=0.54, and Re_ω =456.

7 Acknowledgements

The authors would like to thank Steve Hummel of Hewlett Packard for many valuable discussions and information during the course of this study. This work was supported by the U.S. Department of Energy.

References

[1] G. Evans and R. Greif, A Numerical Model of the Flow and Heat Transfer in a Rotating Disk Chemical Vapor Deposition Reactor, *Journal of Heat Transfer* **109**, 928-935 (1987).

[2] G. Evans and R. Greif, Effects of Boundary Conditions on the Flow and Heat Transfer in a Rotating Disk Chemical Vapor Deposition Reactor, *Numerical Heat Transfer* **12**, 243-252 (1987).

[3] S. Patnaik, R. A. Brown, and C. A. Wang, Hydrodynamic Dispersion in Rotating-Disk OMVPE Reactors: Numerical Simulation and Experimental Measurements, *J. Crystal Growth* **96**, 153-174 (1989).

[4] D. I. Fotiadis, S. Kieda, and K. F. Jensen, Transport Phenonema in Vertical Reactors for Metalorganic Vapor Phase Epitaxy I. Effects of Heat Transfer Characteristics, Reactor Geometry, and Operating Conditions, *J. Crystal Growth* **102**, 441-470 (1990).

[5] S. C. Palmateer, S. H. Groves, C. A. Wang, D. W. Weyburne, and R. A. Brown, Use of Flow Visualization and Tracer Gas Studies for Designing an InP/InGaAsP OMVPE Reactor, *J. Crystal Growth* **83**, 202-210 (1987).

[6] W. S. Winters, G. H. Evans, and R. Greif, Mixed Binary Convection in a Rotating Disk Chemical Vapor Deposition Reactor, *Int. J. Heat and Mass Transfer* accepted for publication (1996).

[7] W. S. Winters, G. H. Evans, and R. Greif, A Two-Dimensional Numerical Model of Gas Mixing and Deposition in a Rotating Disk CVD Reactor, *CVD XIII. Proceedings of the 13th Int. Conf. on CVD*, eds. T. M. Besmann et al., The Electrochemical Society, Inc., Pennington, NJ, 89-94 (1996).

[8] G. H. Evans and R. Greif, Forced Flow near a Heated Rotating Disk: a Similarity Solution, *Numerical Heat Transfer* **14**, 373-387 (1988).

[9] M. E. Coltrin, R. J. Kee, and G. H. Evans, A Mathematical Model of the Fluid Mechanics and Gas-Phase Chemistry in a Rotating Disk Chemical Vapor Deposition Reactor, *J. Electrochem. Soc.* **136**, 819-829 (1989).

[10] F. M. White, *Viscous Fluid Flow*, McGraw-Hill, 164-172 (1974).

[11] J. F. Grcar, The Twopnt Program for Boundary Value Problems, Sandia Report SAND91-8230 (1992).

[12] M. E. Coltrin, R. J. Kee, G. H. Evans, E. Meeks, F. M. Rupley, and J. F. Grcar, SPIN Version 3.83): A Fortran Program for Modeling One-Dimensional Rotating- Disk/Stagnation-Flow Chemical Vapor Deposition Reactors, Sandia Report SAND91-8003 (1991).

[13] S. V. Patankar, *Numerical Heat Transfer and Fluid Flow*, McGraw-Hill (1980).

UNLIMITED RELEASE
INITIAL DISTRIBUTION

P. N. Gadgil
Genus, Inc.
1139 Karlstad Drive
Sunnyvale, CA 94089

R. Greif
Mechanical Engineering Dept.
University of California at Berkeley
Berkeley, CA 94720-1740

W. L. Holstein
DuPont Central Research and
Development
Experimental Station
P. O. Box 80356
Wilmington, DE 19880-0356

S. G. Hummel
Hewlett Packard
3500 Deer Creek Road, MS 26M7
P. O. Box 10350
Palo Alto, CA 94303-0867

S. Joh (10)
Novellus Systems, Inc.
3970 N. First Street, M/S 251
San Jose, CA 95134

R. J. Kee
Engineering Division
Colorado School of Mines
Golden, CO 80401-1887

K. P. Killeen
Hewlett Packard
3500 Deer Creek Road, Bldg. 26M
Palo Alto, CA 94304-1317

M. Ludowise
Hewlett Packard
3500 Deer Creek Road, Bldg. 26M
Palo Alto, CA 94304-1317

E. R. Myers
National Semiconductor
2900 Semiconductor Drive, MS E-100
Santa Clara, CA 95052-8090

M. Peanasky
Hewlett Packard
370 West Trimble Road, MS 91MJ
San Jose, CA 95131-1008

E. J. Smith
Superconductor Technologies, Inc.
460 Ward Drive, Suite F
Santa Barbara, CA 93111-2310

R. Stall
Emcore Corporation
394 Elizabeth Avenue
Somerset, NJ 08873

V. Starov
GaSonics International
2730 Junction Avenue
San Jose, CA 95134-1909

A. Thompson
Emcore Corporation
1431 Newport Way
Seattle, WA 98122-3559

0601 W. G. Breiland, 1126
0601 M. E. Coltrin, 1126
0601 H. K. Moffat, 1126
0601 J. Y. Tsao, 1126

0603 P. Esherick, 1314

9001 T. O. Hunter, 8000
Attn: M. E. John, 8100
A. West, 8200
R. C. Wayne, 8400
A. West, 8600
T. M. Dyer, 8700
L. E. Hiles, 8800
D. L. Crawford, 8900

9054 W. J. McLean, 8300
Attn: C. W. Robinson, 8301
W. Bauer, 8302
L. A. Rahn, 8351
F. P. Tully, 8353
D. R. Hardesty, 8361
R. W. Carling, 8362
R. J. Gallagher, 8366

9042 G. H. Evans, 8345 (10)

9042 C. M. Hartwig, 8345

9042 W. S. Winters, 8345

0841 P. J. Hommert, 9100
Attn: R. D. Skocypec, 9102
W. L. Hermina, 9111
A. C. Ratzel, 9112

9021 Tech. Communications Dept., 8515
Attn: for OSTI (10)

9021 Tech. Communications, 8815

0899 Tech. Library, 4414 (4)

9018 Central Tech. Files, 8940-2 (3)